

## Article

# Dynamic Compression-Bending Performance of Concrete-Filled Steel Tubular Columns under Lateral Impact

Man Xu <sup>1</sup>, Zhichao Ding <sup>1</sup>, Xianjuan Hao <sup>2</sup> and Shan Gao <sup>3,\*</sup> 

<sup>1</sup> School of Civil Engineering and Transportation, Northeast Forestry University, Harbin 150040, China; xuman306@126.com (M.X.)

<sup>2</sup> Design and Development Department, Center International Group Co., Ltd., Beijing 100176, China

<sup>3</sup> Key Lab of Structures Dynamic Behavior and Control of the Ministry of Education, Harbin Institute of Technology, Harbin 150090, China

\* Correspondence: gaoshan@hit.edu.cn

**Abstract:** In this paper, a finite element model of concrete-filled steel tubular (CFST) columns under compression and lateral impact is developed and validated against previous experiments. After analyzing the influence of axial compression on the impact performance of CFST columns, the effects of eccentricity, material strength, and steel ratio on the dynamic compression-bending performances of CFST columns subjected to lateral impact are discussed. The simulated results show that at different axial compression ratios, CFST columns show overall bending failure under lateral impact. The axial force ratio below 0.2 shows a positive effect on the impact resistance of CFST columns, otherwise the axial force would degrade the impact resistance of CFST columns. Eccentricity has a negative effect on the dynamic compression-bending performance of CFST columns. The increase in the concrete strength has little effect on the dynamic compression-bending performance of the CFST columns under lateral impact and eccentric compression. The increases in steel strength and steel ratio can improve the dynamic compression-bending performances of the CFST columns under lateral impact and eccentric compression. Even though the prediction formula for the dynamic compression-bending performance of CFST columns shows good fitness with the simulated results, it is modified to have sufficient strength reserves for design applications.



**Citation:** Xu, M.; Ding, Z.; Hao, X.; Gao, S. Dynamic Compression-Bending Performance of Concrete-Filled Steel Tubular Columns under Lateral Impact. *Buildings* **2023**, *13*, 2289. <https://doi.org/10.3390/buildings13092289>

Academic Editors: Antonio Caggiano and Binsheng (Ben) Zhang

Received: 5 August 2023

Revised: 1 September 2023

Accepted: 5 September 2023

Published: 8 September 2023



**Copyright:** © 2023 by the authors. Licensee MDPI, Basel, Switzerland. This article is an open access article distributed under the terms and conditions of the Creative Commons Attribution (CC BY) license (<https://creativecommons.org/licenses/by/4.0/>).

**Keywords:** lateral impact; eccentricity; CFST column; compression-bending performance; dynamic

## 1. Introduction

Due to the advantages of fast construction, high resistance, and good economy, concrete-filled steel tubular (CFST) structures are increasingly being adopted for high-rise buildings, bridge piers, and other infrastructures [1]. Therefore, the damage to the CFST structures under exceptional impact may result in catastrophic results and massive casualties.

Research on the impact resistance of CFST structures has received increasing attention from engineers and researchers. Zhang [2] studied the mechanical properties of CFST columns with different tube thicknesses through axial impact tests and finite element simulations. The steel ratio and material strength were directly proportional to the impact resistance of CFST. Li et al. [3] studied the dynamic mechanical properties of CFST short columns through the axial impact tests. Zheng [4] studied the concrete-filled steel tubes by axial impact tests, showing that the concrete-filled steel tubes mainly exhibited oblique shear failure. Mirmomeni et al. [5] studied the size effect of circular CFST short columns under axial impact and proposed an empirical formula related to the size and strain rate. Qu et al. [6] used LS-DYNA to simulate the lateral dropping hammer tests on concrete-filled steel tubes and obtained a simplified analysis model based on the results of finite element analysis and rigid-plastic theory. Liu [7] concluded that the increase in the thickness of the steel tube increased the peak value and the platform value of the impact force of the

circular concrete-filled steel tubes. Han et al. [8] carried out lateral impact tests on circular high-strength concrete-filled steel tubes and hollow steel tubes, and proposed a simplified formula related to steel strength, steel ratio, section size, and impact velocity. Hou et al. [9] used the finite element method to study the life cycle and residual bearing capacity of concrete-filled steel tubes from the aspects of preloading and residual stresses. Yang [10] concluded that the impact force platform values of square high-strength concrete-filled steel tubes under lateral impact were almost unaffected by impact energy. Wang et al. [11] found that the CFST specimens experienced an obvious local response stage before cracking. Through a numerical parametric analysis, Gao et al. [12] proposed the prediction formulas for the residual resistance of square CFST columns under repeated lateral impacts. In addition, FRP composites are supposed to provide benefits for the impact resistance of CFST columns [13,14].

It can be seen that most of the present research focuses on the dynamic response, lateral resistance, and residual axial resistance of CFST columns under lateral impact. Even though some tests considered the axial force on CFST columns while conducting lateral impact, the axial force is only considered as pre-loading conditions, namely, the axial compression ratio, instead of being combined with bending moment. The dynamic compression-bending performance, namely, the  $N$ - $M$  relationship curve of CFST under lateral impact, has never been mentioned. The dynamic compression-bending performance of CFST under lateral impact is rather meaningful for practical design and application since most CFST columns in frames are under the service loading combination of axial force and bending moment, which are vulnerable under lateral impact.

In this paper, the numerical model of the CFST columns under the coupling of axial force–lateral impact is developed by using ABAQUS and validated against the experimental data from previous research. The effects of eccentricity, material strength, and steel ratio on the dynamic compression-bending performances of CFST columns under lateral impact are investigated. Based on the simulated results, a compression-bending relation formula for CFST columns under lateral impact is proposed aiming at practical design.

## 2. Development and Validation of the Finite Element Model

### 2.1. Elements

The finite element model (FEM) consisting of a steel tube, core concrete, and a dropping hammer is shown in Figure 1. The steel tube and core concrete are modeled by using the ‘C3D8R’ element, namely, a 3D eight-node linear reduced integral element with a mesh size of 50 mm which is determined by a trial running. The ‘R3D4’ element, namely, a 3D four-node bilinear quadrilateral element, is used to simulate a dropping hammer, since the deformation of the hammer is ignored.

### 2.2. Boundary Conditions and Contacts

To facilitate the application of boundary conditions, impact, and axial force, the reference points are set at the ends of the model and the dropping hammer, respectively. The reference point at one end of the model is set as a fixed constraint, namely,  $U_x = U_y = U_z = UR_x = UR_y = UR_z = 0$ . The reference point RP1 on the top of the column is constrained except for the  $y$ -direction translation degree of freedom, namely,  $U_x = U_z = UR_x = UR_y = UR_z = 0$ . In addition, the position of the reference point RP1 changes as the eccentricity of the member. Regardless of the free-falling process, the dropping hammer is placed in the initial position of contact with the specimen, whilst the mass and impact velocity of the dropping hammer are applied to the reference point at the dropping hammer. The impact velocity of the dropping hammer is taken from the corresponding free-fall velocity from the impact height calculated by  $V = \sqrt{2gh}$ , where  $h$  is the impact height by ignoring the energy loss during the falling process of the hammer.

The interface contact of the finite element model is defined as “general contact”. For the steel tube and dropping hammer, the tangential direction of contact is defined as

“frictionless”. The cohesive force between the steel tube and the concrete is calculated by Equation (1) from Ref. [15] as:

$$\tau_{bond} = 0.75[2.314 - 0.0195(B/t_s)] \tag{1}$$

where  $\tau_{bond}$  is the bond stress of the contact surface,  $B$  is the concrete side length in the square concrete-filled steel tube, and  $t_s$  is the thickness of the steel tube. If the shear stress of the contact surface is less than  $\tau_{bond}$ , there is no relative slip at the interface. At this time, the Coulomb friction model is used to characterize the relative slip between the two and the corresponding friction coefficient is 0.6 [16].

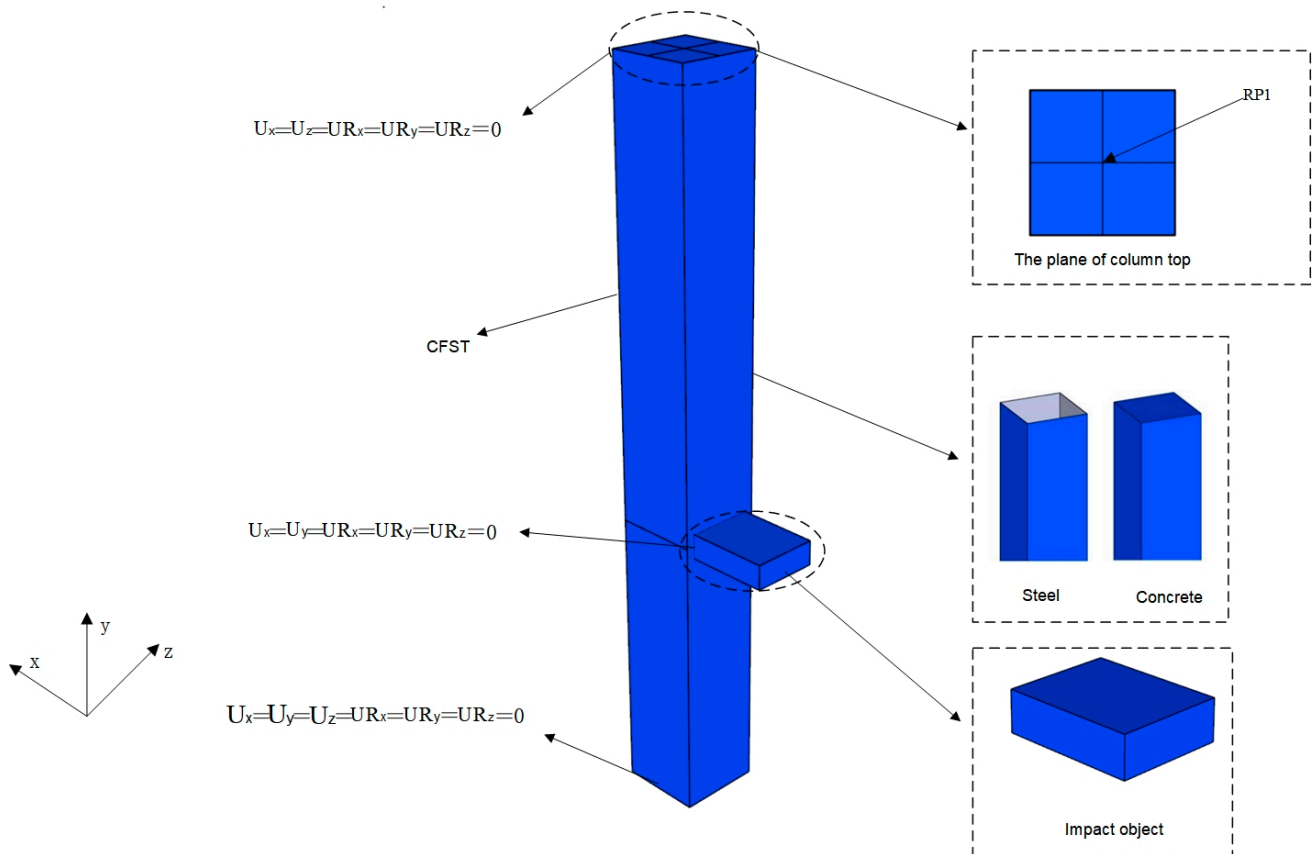


Figure 1. Finite element model.

### 2.3. Constitutive Relationship of Material

#### 2.3.1. Steel

Based on the previous studies from the authors’ research group [12], the static material model of steel shows little effect on the performance of CFST columns under lateral impact load. Since normal-strength low-carbon steel is used in this study, the secondary plastic flow model by Han [17] is used as shown in Figure 2. The specific expression is described by Equation (2), where  $f_p$ ,  $f_v$ , and  $f_u$  represent the proportional limit, yield strength, and tensile strength of the steel, respectively.

$$\sigma_s = \begin{cases} E_s \epsilon_s & \epsilon_s \leq \epsilon_e \\ -A\epsilon_s^2 + B\epsilon_s + C & \epsilon_e < \epsilon_s \leq \epsilon_{e1} \\ f_y & \epsilon_{e1} < \epsilon_s \leq \epsilon_{e2} \\ f_y \left(1 + 0.6 \frac{\epsilon_s - \epsilon_{e2}}{\epsilon_{e3} - \epsilon_{e2}}\right) & \epsilon_{e2} < \epsilon_s \leq \epsilon_{e3} \\ 1.6f_y & \epsilon_s > \epsilon_{e3} \end{cases} \tag{2}$$

where  $\varepsilon_e = 0.8f_y/E_s$ ,  $\varepsilon_{e1} = 1.5\varepsilon_e$ ,  $\varepsilon_{e2} = 10\varepsilon_{e1}$ ,  $\varepsilon_{e3} = 100\varepsilon_{e1}$ ,  $A = 0.2f_y/(\varepsilon_{e1} - \varepsilon_e)^2$ ,  $B = 2A\varepsilon_{e1}$ , and  $C = 0.8f_y + A\varepsilon_e^2 - B\varepsilon_e$ .

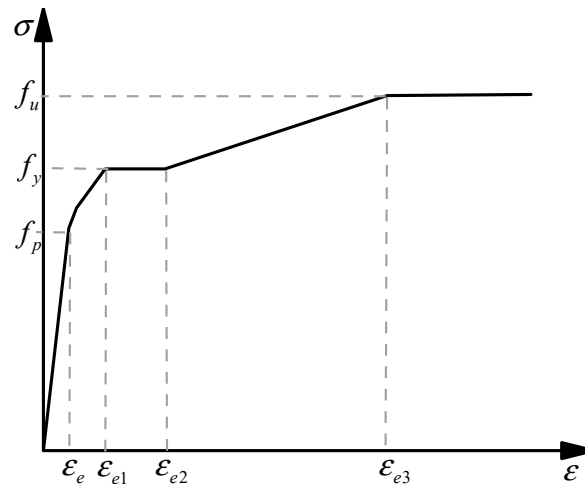


Figure 2. Stress–strain relationship curve for steel.

The Cowper–Symonds model is used in the simulation due to its suitability for the calculation of dynamic problems with low strain rates. The model is expressed by Equation (3), where  $\dot{\varepsilon}$  is the strain rate of steel,  $\sigma_d$  is the stress at the strain rate  $\dot{\varepsilon}$  of steel,  $\sigma_s$  is the stress value of steel under static force, and  $D$  and  $P$  are the material fitting parameters and could be taken as  $4945 \text{ s}^{-1}$  and 2.696, respectively [18–20].

$$\sigma_d/\sigma_s = 1 + (\dot{\varepsilon}/D)^{1/p} \quad (3)$$

### 2.3.2. Concrete

The Concrete Damaged Plasticity (CDP) model from ABAQUS library is used to describe the mechanical behavior of concrete. The dilation angle, flow potential eccentricity, the ratio of the compressive strength under biaxial loading to the uniaxial compressive strength,  $f_{b0}/f_{c0}$ , the ratio of the second stress invariant on the tensile meridian to that on the compressive meridian,  $K$ , and the viscosity coefficient of concrete are set to  $30^\circ$ , 0.1, 1.16, 0.667, and 0.0005, respectively [21].

The stress–strain relationship of concrete under uniaxial compression provided in Ref. [17] is adopted, as expressed by Equation (4):

$$y = \begin{cases} 2x - x^2 & x \leq 1 \\ \frac{x}{\beta_0(x-1)^\eta + x} & x > 1 \end{cases} \quad (4)$$

where  $x = \varepsilon/\varepsilon_0$ ,  $y = \sigma/\sigma_0$ ,  $\sigma_0 = f_c'$ ,  $\varepsilon_0 = \varepsilon_c + 800 \cdot \zeta^{0.2} \cdot 10^{-6}$ ,  $\varepsilon_c = (1300 + 12.5f_c')10^{-6}$ ,  $\eta = 1.6 + 1.5/x$ ,  $\beta_0 = \frac{(f_c')^{0.1}}{1.2\sqrt{1+\zeta}}$ .

The uniaxial tensile stress–strain relationship of concrete is expressed by Equation (5):

$$y = \begin{cases} 1.2x - 0.2x^6 & x \leq 1 \\ 0.31\sigma_p^2(x-1)^{1.7} + x & x > 1 \end{cases} \quad (5)$$

where  $x = \varepsilon/\varepsilon_p$ ,  $y = \sigma/\sigma_p$ ,  $\sigma_p = 0.26 \times (1.25f_c')^{2/3}$ ,  $\sigma_p$  is the peak tensile stress of concrete, and  $\varepsilon_p = 43.1 \mu\varepsilon$  is the strain value corresponding to the peak tensile stress of concrete.

The effect of the strain rate of concrete is considered by using the relationship between DIF (dynamic increase factor) and strain rate  $\dot{\varepsilon} = 3 \times 10^{-5} \sim 300 \text{ s}^{-1}$  of concrete provided by CEB-FIP (1988) [22].

- (1) Equation (6) is used for the concrete under dynamic compression:

$$DIF = \frac{f_{cd}}{f_{cs}} = \begin{cases} \left(\frac{\dot{\epsilon}}{\dot{\epsilon}_s}\right)^{1.026\alpha_s} & \dot{\epsilon} \leq 30s^{-1} \\ \gamma_s \left(\frac{\dot{\epsilon}}{\dot{\epsilon}_s}\right)^{1/3} & \dot{\epsilon} > 30s^{-1} \end{cases} \quad (6)$$

where  $f_{cs}$  and  $f_{cd}$  are the static compression strength and dynamic compression strength respectively,  $\gamma_s = 10^{(6.156\alpha_s - 2.0)}$ ,  $\alpha_s = (5 + 9f_{cs}/f_{co})^{-1}$ ,  $\dot{\epsilon}_s = 30 \times 10^{-6}s^{-1}$  (quasi-static strain rate), and  $f_{co} = 10$  MPa.

- (2) Equation (7) is used for the concrete under dynamic tension:

$$DIF = \frac{f_{td}}{f_{ts}} = \begin{cases} \left(\frac{\dot{\epsilon}}{\dot{\epsilon}_s}\right)^{1.016\delta} & \dot{\epsilon} \leq 30s^{-1} \\ \beta \left(\frac{\dot{\epsilon}}{\dot{\epsilon}_s}\right)^{1/3} & \dot{\epsilon} > 30s^{-1} \end{cases} \quad (7)$$

where  $\delta = (10 + f_{cs}/f_{co})^{-1}$ ,  $\beta = 10^{7.11\delta - 2.33}$ ,  $f_{ts}$ , and  $f_{td}$  are the static tensile strength and dynamic tensile strength, respectively,  $\dot{\epsilon}_s = 30 \times 10^{-6}s^{-1}$  (quasi-static strain rate), and  $f_{co} = 10$  MPa.

#### 2.4. Model Validation

The results of the axial force–impact coupling tests from Ref. [23] are used to validate the finite element model. The steel tube used in the tests was cut from a pre-fabricated cold-formed square hollow section with an average thickness of 2.45 mm. The average yield strength, tensile strength, elastic modulus, and Poisson's ratio of steel are 370.8 MPa, 446.5 MPa,  $1.98 \times 10^5$  N/mm<sup>2</sup>, and 0.267, respectively. The compressive strength and elastic modulus of concrete are 53.9 MPa and  $3.29 \times 10^4$  MPa, respectively. The relevant test information is listed in Table 1 and more detailed information can be found in Ref. [23].

**Table 1.** Details of the test specimens in Ref. [23].

Group	Specimen Number	Axial Compression Ratio	Length/mm	Cross Section/mm	Hammer Weight/kg	Impact Velocity/(m/s)
1	NC-0-6	0	1800	$B \times t = 100 \times 2.45$	238	10.85
2	NC-0.15-6	0.15	1800	$B \times t = 100 \times 2.45$	238	10.85
3	NC-0.3-6	0.3	1800	$B \times t = 100 \times 2.45$	238	10.85

As shown in Figure 3, the impact force–time history curves of the three specimens in Table 1 mainly experienced three stages: oscillation stage, stable stage, and attenuation stage. From the impact force–time history curves for different axial compression ratios, it can be concluded that the impact force platform value gradually decreases as the axial force increases. This is due to the increased ability of the column to resist lateral impact under axial force within a certain range, resulting in a decrease in the deflection and the impact force platform value. In general, the overall trends of the curves and the magnitudes of the feature values are similar, indicating that the finite element models can accurately reflect the effect of axial force on the impact performance of CFST columns.

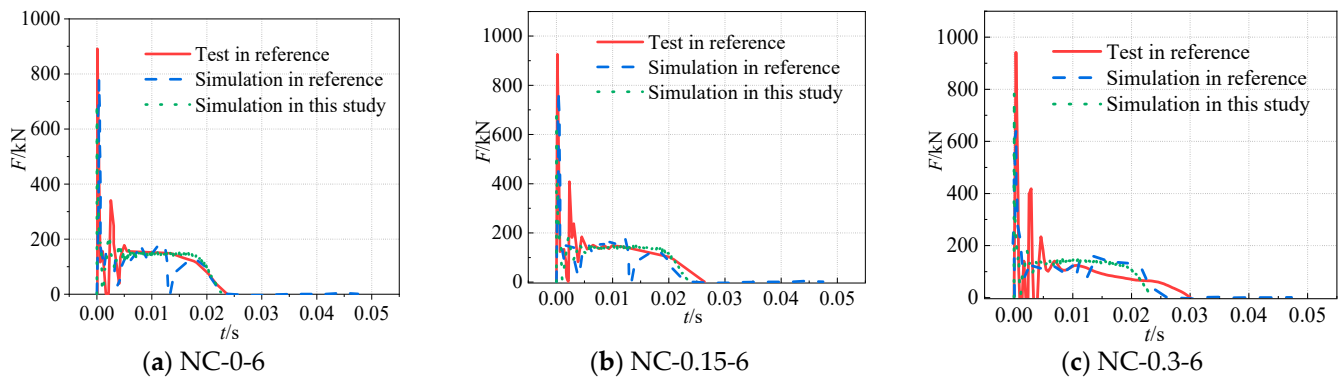


Figure 3. Comparisons of the simulated and tested results.

### 3. Effect of the Axial Compression Ratio on Impact Performance of the CFST Columns

Axial compression ratio is an important parameter affecting the lateral impact resistance of CFST columns [24,25]. In this section, the axial compression ratio  $n$  is taken as 0, 0.1, 0.2, 0.3, 0.4, and 0.5 whilst the steel tube is Q345, the concrete is C60, and the eccentricity is zero. According to the previous studies from the authors' research group [12], the cross-sectional shape for the same cross-sectional area and the shape of the drop hammer are also expected to have little effect on the lateral impact performance of CFST columns. Therefore, the size of the dropping hammer is set as 120 mm × 320 mm × 400 mm and only a square section tube is used in the model. Besides, aiming to provide a reference for practical design and application, only a full-scale height of square CFST is used in this study. The detailed parameters of the specimens are given in Table 2.

Table 2. Parameters and results of the axial compression specimens.

Axial Compression Ratio $n$	$B \times t/\text{mm}$	Specimen Height $H/\text{m}$	Impact Mass $m/\text{t}$	Impact Speed $V/\text{m/s}$	Impact Height $H/\text{m}$	$F_{\max}/\text{kN}$	$F_{\text{stab}}/\text{kN}$	$\Delta/\text{mm}$
0	400 × 10	3.5	1.856	16.67	1.385	5238.78	2252.91	87.95
0.1						5427.20	2371.83	84.93
0.2						5386.24	2268.79	87.07
0.3						5230.59	1997.79	94.93
0.4						5140.48	1405.63	123.35
0.5						5509.12	393.03	545.46

Note:  $F_{\max}$  is the maximum value of the impact force,  $F_{\text{stab}}$  is the platform value of the impact force, and  $\Delta$  is the peak deflection of the concrete-filled steel tubular column.

The platform value of the impact force of the models is calculated by using Equation (8) from Ref. [10]:

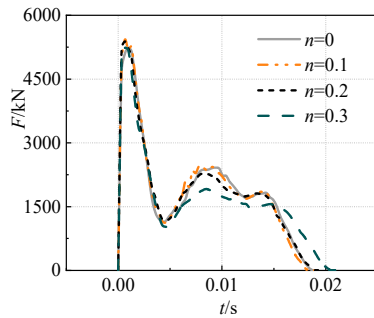
$$F_p = \frac{\int_{t_0}^{t_2} F(t) dt}{t_2 - t_0} \quad (8)$$

where  $F(t)$  is the impact force,  $t_0$  is the moment when the impact force reaches the peak value, and  $t_2$  is the moment when the deflection reaches the peak value.

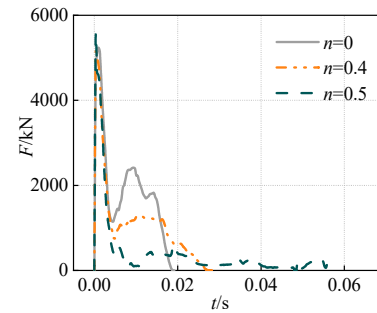
#### 3.1. Impact Force Curve

From Figure 4a,b, it can be seen that as the axial compression ratio increases, the duration of impact force gradually increases. As shown in Figure 4c, the impact platform value with an axial compression ratio of 0.1 is greater than that without axial compression. For an axial compression ratio of 0.2, the impact platform value is almost the same as that without axial compression. With the increase in the axial compression ratio, the impact platform values of the specimens under axial forces are generally lower than those without axial forces. As shown in Figure 4d, the peak impact force of the CFST column is less

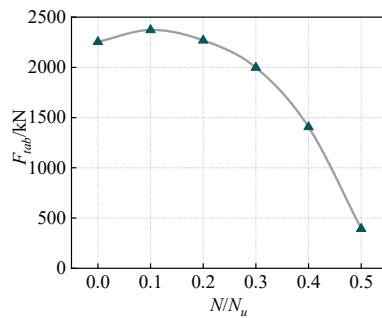
affected by the axial force, since the time consumed at the beginning of the impact is very short and the axial compression hardly affects the peak impact force between the impact body and the column. When  $n > 0.2$ , the increase in the axial force accelerates the bending of the CFST column. In other words, increasing the axial force leads to more obvious second-order effects and decreases the impact resistance of CFST columns.



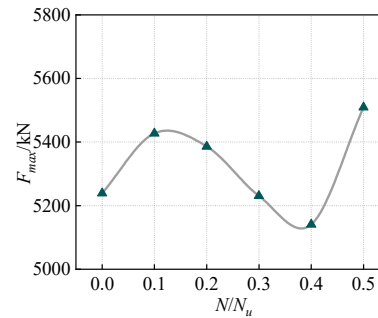
(a) Impact force–time history curves for  $n = 0, 0.1, 0.2,$  and  $0.3$ .



(b) Impact force–time history curves for  $n = 0, 0.4,$  and  $0.5$ .



(c) Relationship between the impact platform and axial compression ratio.

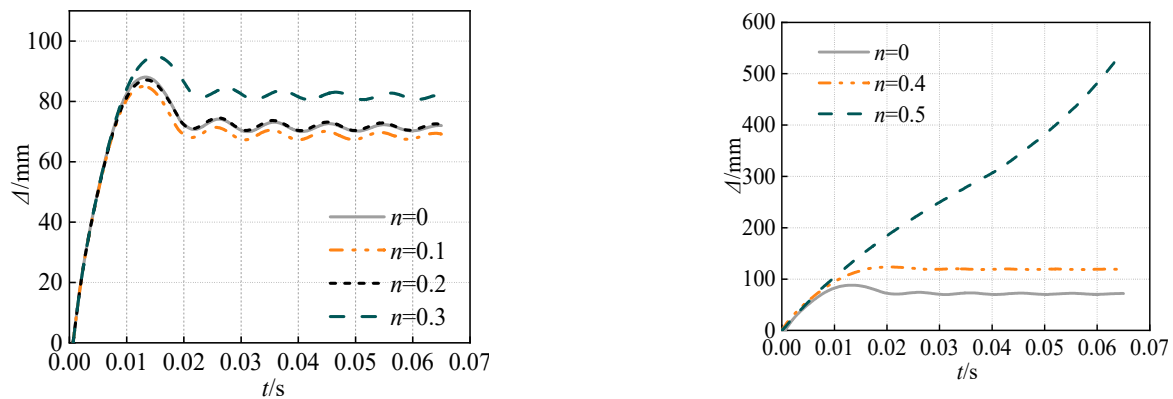


(d) Relationship between the maximum impact force and axial compression ratio.

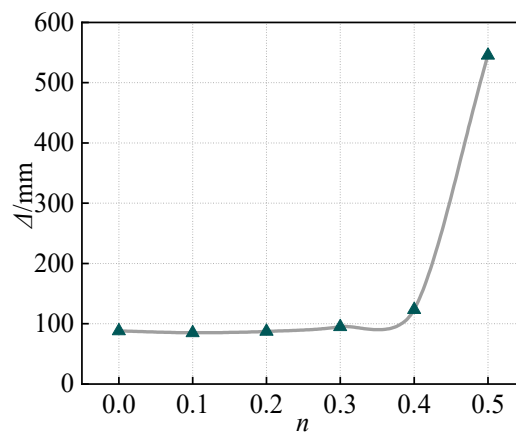
**Figure 4.** Impact force-related curves.

### 3.2. Deflection Curves

It can be seen from Figure 5a,b that when the axial compression ratio is relatively low, the lateral deflection curves of the CFST column show oscillations after reaching the peak values. As the axial compression ratio increases, the oscillation amplitudes weaken or even disappear. The deflection of the member with the axial compression ratio of 0.1 is lower than that without axial force, decreasing from 87.95 mm to 84.93 mm, indicating that the axial force enhances the sectional resistance of the member. For an axial compression ratio of 0.2, the peak values of the deflection curves are almost the same as those without axial force. At the axial compression ratio of 0.5, the lateral deflection is 545.46 mm, and the column is damaged. Since the axial force accelerates the bending of the member, the deflection of the member increases rapidly under the lateral impact, as shown in Figure 5c.



(a) Lateral deflection–time history curves for  $n = 0, 0.1, 0.2$ , (b) Lateral deflection–time history curves for  $n = 0, 0.4$ , and 0.5.

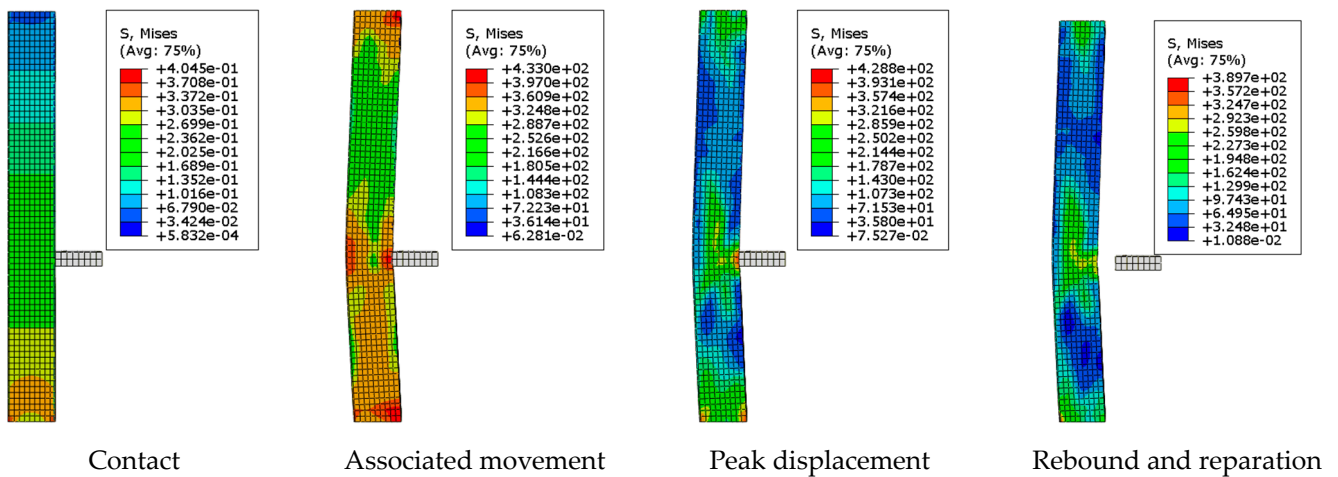


(c) Relationship between the peak deflection and axial compression ratio.

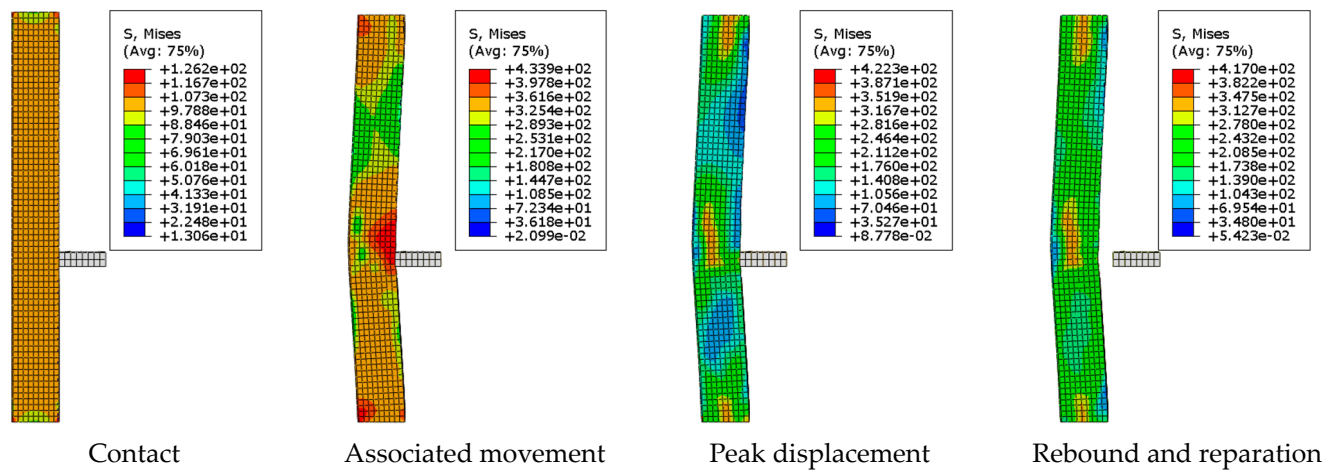
**Figure 5.** Deflection-related curves.

### 3.3. Stress Contours

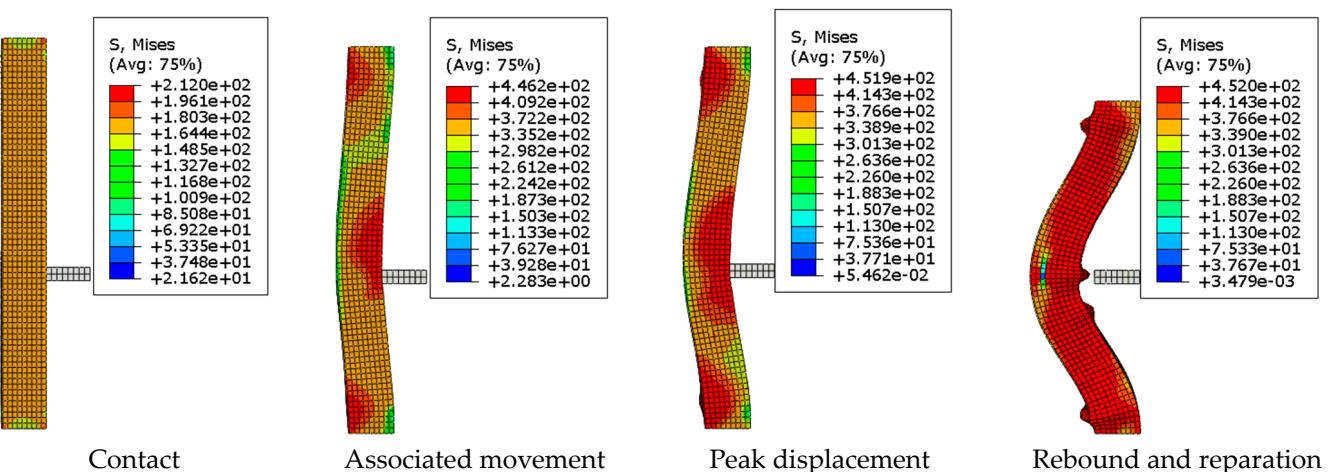
As shown in Figure 6a, it can be seen that the stress of the CFST column without axial force is almost zero before the lateral impact begins. With the increase in the axial compression ratio, the stress of the entire column increases, as shown in Figure 6b,c. Under the action of lateral impact, the impact part and both ends of the column are higher stress areas. With the increase in the axial compression ratio, the range of the high-stress area expands. As for the continuous effect of the impact, the high-stress regions at the impact site and the two ends of the column expand successively, and the overall bending deformation range of the CFST column also increases. During the rebound and reparation stage, the impacted part and the backs of the two ends of the column appear to buckle, and typical overall bending damage occurs in the column.



(a) Stress distributions of the CFST columns under compression with the axial compression ratio  $n = 0$ .



(b) Stress distributions of the CFST columns under compression with the axial compression ratio  $n = 0.3$ .



(c) Stress distributions of the CFST columns under compression with the axial compression ratio  $n = 0.5$ .

Figure 6. Comparison of the stress distributions of the CFST columns under different axial compression ratios.

#### 4. Parametric Studies on the Dynamic Compression-Bending Performances of the CFST Columns

##### 4.1. Model Introduction

To investigate the dynamic compression-bending performances of the eccentric compression CFST columns under lateral impact, the eccentricity, concrete strength, steel strength, and steel ratio of CFST columns are considered. The section of the steel tube is  $B \times B = 400 \text{ mm} \times 400 \text{ mm}$  whilst the tube thicknesses are 5 mm, 10 mm, and 15 mm, respectively. The overall height  $H$  of the column is 3500 mm. The steel tube is made of Q235, Q345, and Q390 steel, and the core concrete is made of C40, C50, and C60 concrete grades. The eccentricities are set as 0 mm, 35 mm, 45 mm, and 55 mm, respectively. The basic parameters of the specimens are given in Table 3. The simulated results are summarized in Table 4. The formula for calculating the axial compression resistances of square CFST columns is Equation (9):

$$N \leq (1/\gamma)N_u \quad (9)$$

$$N_u = fA_s + f_cA_c \quad (10)$$

where  $f$  is the compressive strength of the steel tube,  $f_c$  is the axial compressive strength of the core concrete,  $A_s$  is the cross-sectional area of the steel tube,  $A_c$  is the cross-sectional area of the core concrete,  $N$  is the design value of the axial resistance,  $N_u$  is the sectional compressive-bearing capacity, and  $\gamma$  is the coefficient according to Technical Regulations for Rectangular Concrete-Filled Steel Structures.

**Table 3.** Detailed information of the specimens.

Specimen Number	Column Section Size/mm	Concrete	Steel	Eccentric Distance/mm	Steel Ratio/ $\alpha$
CF1	400 × 400 × 10	C60	Q345	0	0.108
CF2	400 × 400 × 10	C50	Q345	55	0.108
CF3	400 × 400 × 10	C40	Q345	55	0.108
CF4	400 × 400 × 10	C60	Q235	55	0.108
CF5	400 × 400 × 10	C60	Q345	55	0.108
CF6	400 × 400 × 10	C60	Q390	55	0.108
CF7	400 × 400 × 10	C60	Q345	35	0.108
CF8	400 × 400 × 10	C60	Q345	45	0.108
CF9	400 × 400 × 5	C60	Q345	55	0.052
CF10	400 × 400 × 15	C60	Q345	55	0.169

**Table 4.** Calculations of the bending moment  $M$  of the eccentric compression CFST columns under impact.

Number	$n = 0$	$n = 0.1$	$n = 0.2$	$n = 0.3$	$n = 0.4$	$n = 0.5$	$n = 0.6$	$n = 0.7$	$n = 0.8$	$n = 0.9$
CF2	942.7	909.3	828.0	714.7	562.9	467.9	377.8	274.6	177.0	98.0
CF3	956.0	920.2	836.3	722.8	602.6	508.6	416.4	315.6	220.6	143.9
CF4	961.2	924.7	849.5	711.1	622.6	527.7	427.6	445.3	245.8	160.1
CF5	704.3	678.9	604.8	522.2	442.2	368.6	293.3	217.8	160.9	36.1
CF6	1059.6	1026	94.3	806.3	689.4	495.3	495.9	397.8	300.0	196.2
CF7	952.4	953.4	921.5	847.0	738.2	607.6	483.5	351.8	254.1	177.8
CF8	951.2	944.9	893.1	823.0	693.8	561.5	409.9	295.8	188.7	105.4
CF9	540.2	550.4	472.2	357.3	293.0	227.5	133.4	85.2	56.5	45.4
CF10	1297.3	1282.0	1216	1128.2	1025.1	892.8	731.4	560.0	446.2	332.8

The bending capacity of the models is calculated according to Equation (11) [26], where the bending moment is extracted from the impact position section of the models:

$$M_u = \gamma_m W_{sc} f_{sc} \quad (11)$$

where  $f_{sc}$  is the compressive strength of the concrete-filled steel tube,  $\gamma_m$  is the coefficient of plastic development, and  $W_{sc}$  is the section modulus of the bending member.

## 4.2. Analysis of the Results

### 4.2.1. Eccentricity

To investigate the influence of eccentricity on the dynamic compression-bending performances of eccentric compression CFST columns under lateral impact, the eccentricity values of  $e = 35$  mm, 45 mm, and 55 mm are adopted. It can be seen from Figure 7 that the dynamic  $N/N_u - M/M_u$  curves for different eccentricities show decreasing trends. The curves are divided into two parts at  $N/N_u = 0.6$ . Even as the normalized curves, the increase in the eccentricity would decrease the enveloping areas of the dynamic  $N/N_u - M/M_u$  curves of the CFST columns, indicating the worse impact resistances.

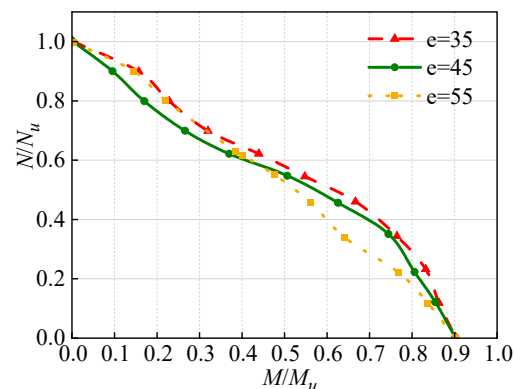


**Figure 7.** Effect of eccentricity on the dynamic  $N/N_u - M/M_u$  curves.

### 4.2.2. Concrete Strength

To investigate the influence of concrete strength on the dynamic compression-bending performances of eccentric compression CFST columns under lateral impact, C40, C50, and C60 concrete grades are adopted. It can be seen from Figure 8 that the dynamic  $N/N_u - M/M_u$  curves with different concrete strengths show decreasing trends. At  $M/M_u = 0.55$ , the three curves almost intersect at one point. The  $N/N_u - M/M_u$  curves for the eccentric compression CFST columns indicate that the increase in the concrete strength has a minor effect on the bending capacity of the columns. This is because the core concrete in the concrete-filled steel tube contributes little to the flexural strength of the member sections and plays a supporting role under lateral impact.

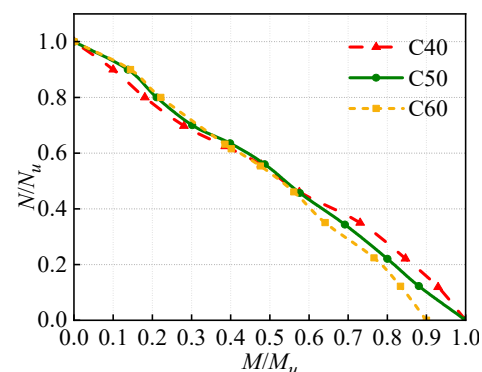


**Figure 8.** Effect of concrete strength on the dynamic  $N/N_u - M/M_u$  curves.

### 4.2.3. Steel Strength

To investigate the influence of steel strength on the dynamic compression-bending performances of eccentric compression CFST columns under lateral impact, Q235, Q345, and Q390 steel grades are selected. As can be seen from Figure 9, the dynamic  $N/N_u - M/M_u$

curves with different steel strengths show decreasing trends. At the beginning of the curve, the CFST column with Q235 steel has the smallest  $M/M_u$  value. With the increasing steel strength, the restraint effect on the core concrete is enhanced and thus it has a better ability to delay deformation.

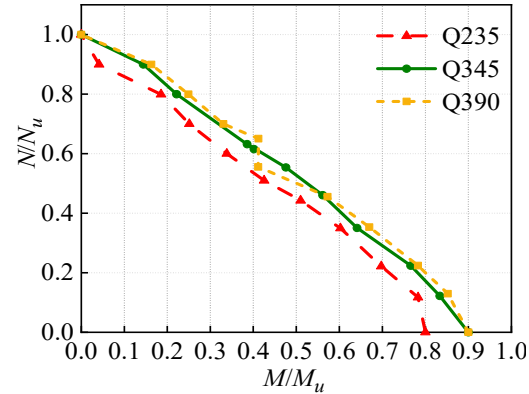


**Figure 9.** Effect of steel strength on the dynamic  $N/N_u$ - $M/M_u$  curves.

#### 4.2.4. Steel Ratio

To investigate the influence of steel ratio on the dynamic compression-bending performances of eccentric compression CFST columns under the lateral impact, the steel ratios of  $\alpha = 0.052$ ,  $0.108$ , and  $0.169$  are adopted. It can be seen from Figure 10 that the  $M/M_u$  values increase significantly with the increasing steel ratio, indicating better dynamic compression-bending performances of the model. This is because increasing the steel ratio improves the resistance and stiffness of the columns which can largely delay the deformation.

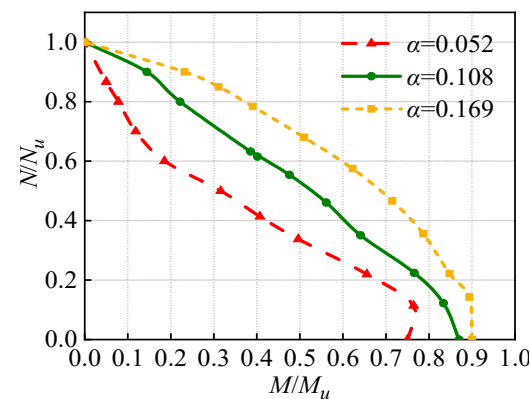


**Figure 10.** Effect of steel ratio on the dynamic  $N/N_u$ - $M/M_u$  curves.

### 5. Dynamic Compression-Bending Formula for the CFST Columns

According to the above parameter analysis, the dynamic compression-bending formula for the eccentric compression CFST columns can be divided into two parts:

When  $(N/N_u) \leq 0.2$ ,

$$a \left( \frac{N}{N_u} \right) + \left( \frac{M}{M_u} \right) = b \quad (12)$$

Through the analysis of the previous results, the fitting coefficients  $a$  and  $b$  are  $0.7$  and  $1.0$ , respectively, so the compression-bending formula of CFST columns can be expressed as Equation (13):

$$0.7 \left( \frac{N}{N_u} \right) + \left( \frac{M}{M_u} \right) = 1 \quad (13)$$

When  $(N/N_u) > 0.2$ ,

$$\left(\frac{N}{N_u}\right)^a + \left(\frac{M}{M_u}\right)^b = 1 \tag{14}$$

Through the analysis of the previous results, the fitting coefficients  $a$  and  $b$  are 1.1 and 1.1, respectively, so the compression-bending formula for CFST columns can be expressed as Equation (15):

$$\left(\frac{N}{N_u}\right)^{1.1} + \left(\frac{M}{M_u}\right)^{1.1} = 1 \tag{15}$$

where  $N$  and  $M$  are the axial force and bending moment of concrete-filled steel tube columns, respectively,  $N_u$  is the axial compressive resistance of CFST columns, and  $M_u$  is the flexural resistance of CFST columns.

From Figure 11, it can be seen that the fitting accuracy of the formula is high with  $R^2 = 0.95$ . To have sufficient strength reserves for the practical design, the fitting formula is modified as Equations (16) and (17). The predicted results from the modified formula are all smaller than the simulated results, indicating the dynamic  $N$ - $M$  strength reserves by using Equations (16) and (17). The differences between the simulated and the predicted results from the modified formulas are approximately 20%.

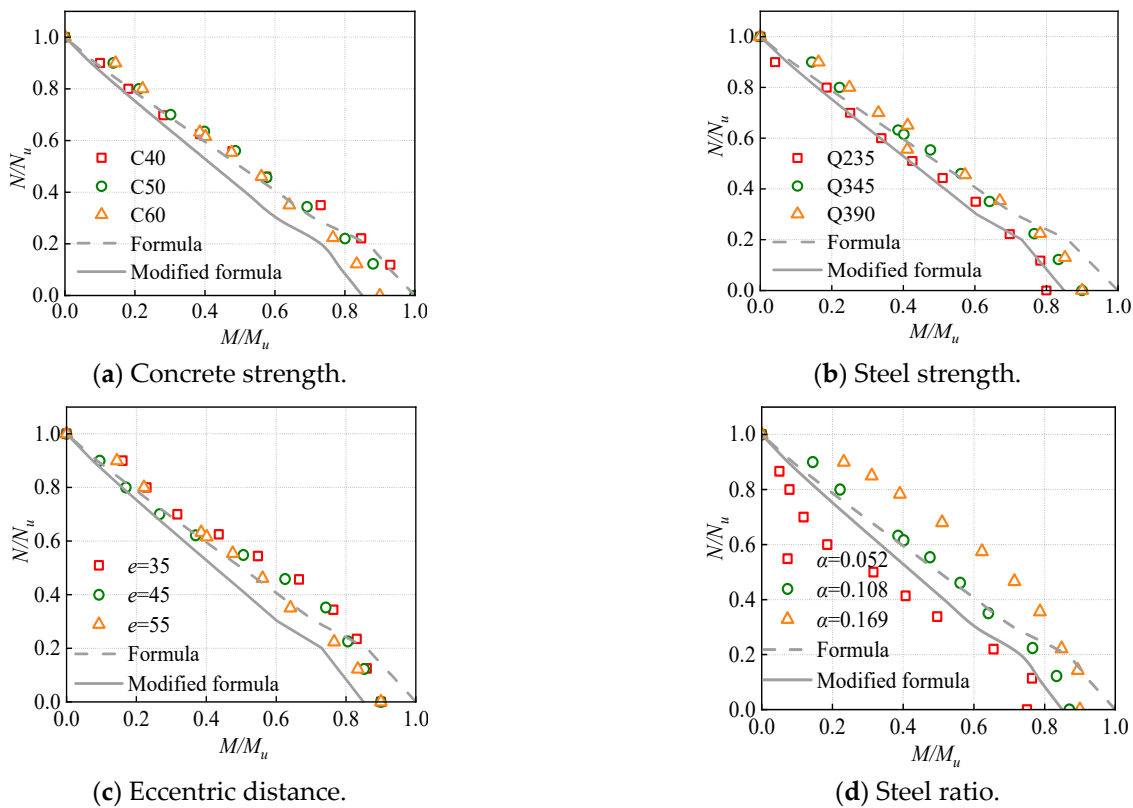


Figure 11. Comparisons of the simulated and predicted results.

When  $(N/N_u) \leq 0.2$ ,

$$0.7\left(\frac{N}{N_u}\right) + \frac{20}{17}\left(\frac{M}{M_u}\right) = 1 \tag{16}$$

When  $(N/N_u) > 0.2$ ,

$$\left(\frac{N}{N_u}\right)^{1.1} + \frac{20}{17}\left(\frac{M}{M_u}\right)^{1.1} = 1 \tag{17}$$

The proposed dynamic compression-bending formula for CFST columns could be used to determine the corresponding internal forces of CFST columns when considering the

impact design. Then the section design of CFST columns under the design service loads and impact load could be conducted by using the most unfavorable internal load combination.

## 6. Conclusions

In this paper, the dynamic compression-bending performances of CFST columns under lateral impact load are studied. Some conclusions are drawn as follows.

- (1) The axial compression ratio of 0.2 is a feature point to evaluate the impact resistance of the CFST column. The axial force ratio shows a positive effect on the impact resistance of CFST columns when less than 0.2, otherwise the axial force would degrade the impact resistance of CFST columns.
- (2) The increase in the steel strength and steel ratio rather than the concrete strength has a positive effect on the dynamic compression-bending performances of eccentric compression CFST columns under impact.
- (3) Based on the simulated results with different parameters, a high-accuracy dynamic compression-bending formula for CFST columns is obtained. The formula is also modified to have a sufficient strength reserve for the practical design.

**Author Contributions:** Methodology, M.X.; Formal analysis, X.H.; Writing—original draft, Z.D.; Writing—review & editing, S.G. All authors have read and agreed to the published version of the manuscript.

**Funding:** The project is supported by the National Natural Science Foundation of China (Grant No. 51908085), Fundamental Research Funds for the Central Universities (Grant No. AUGA5710010322), and The Youth Innovation Team of Shaanxi Universities (Grant No. 21JP138).

**Data Availability Statement:** The raw/processed data required to reproduce these findings can be shared.

**Acknowledgments:** The project is supported by the National Natural Science Foundation of China (Grant No. 51908085), Fundamental Research Funds for the Central Universities (Grant No. AUGA5710010322), and The Youth Innovation Team of Shaanxi Universities (Grant No. 21JP138), which are gratefully acknowledged.

**Conflicts of Interest:** We declare that we do not have any commercial or associative interest that represents any conflict of interest in connection with the work submitted.

## References

1. Han, L.H. *Theory and Practice of Concrete-Filled Steel Tubular Structures*; Science Press: Beijing, China, 2017; pp. 66–110.
2. Zhang, C. *Dynamic Analysis of Concrete-Filled Steel Tubular Columns under Impact Load*; Taiyuan University of Technology: Taiyuan, China, 2005.
3. Li, Z.; Li, B.; Li, Y.G.; Ren, G.P. Discussion on dynamic characteristics of axial impact of concrete-filled steel tubular short columns. *J. Taiyuan Univ. Technol.* **2006**, *4*, 383–385.
4. Zheng, Q. *Experimental Study and Finite Element Analysis on Impact Resistance of Concrete-Filled Steel Tubular Short Columns*; Hunan University: Changsha, China, 2008.
5. Mirmomeni, M.; Heidarpour, A.; Zhao, X.L.; Al-Mahaidi, R. Size-dependency of concrete-filled steel tubes subject to impact loading. *Int. J. Impact Eng.* **2017**, *100*, 90–101. [[CrossRef](#)]
6. Qu, H.; Li, G.; Chen, S.; Sun, J.; Sozen, M.A. Analysis of circular concrete-filled steel tube specimen under lateral impact. *Adv. Struct. Eng.* **2011**, *14*, 941–951. [[CrossRef](#)]
7. Liu, Y.L. *Experimental Study and Numerical Analysis of Lateral Impact Response of Concrete-Filled Steel Tubular Members with Common Constraint Types*; Taiyuan University of Technology: Taiyuan, China, 2005.
8. Han, L.H.; Hou, C.C.; Zhao, X.L.; Rasmussen, K.J.R. Behavior of high-strength concrete-filled steel tubes under transverse impact loading. *J. Constr. Steel Res.* **2014**, *92*, 25–39. [[CrossRef](#)]
9. Hou, C.C.; Han, L.H. Life-cycle performance of deteriorated concrete-filled steel tubular (CFST) structures subject to lateral impact. *Thin-Walled Struct.* **2018**, *132*, 362–374. [[CrossRef](#)]
10. Yang, X.Q. *Dynamic Constitutive Model of Structural Steel and Lateral Impact Resistance of High Strength CFST Square Members*; Harbin Institute of Technology: Harbin, China, 2020.
11. Wang, L.M.; Liu, Y.H.; Zhao, S.C.; Zhao, Y.C.; Kang, X.J. Research on cracking evaluation model and influencing factors of concrete-filled steel tubular members under lateral low-velocity impact. *J. Civ. Eng.* **2022**, *55*, 7–17.

12. Gao, S.; Xu, Y.C.; Zhang, S.M.; Derlatka, A. Performance of square concrete-filled steel tubular columns under repeated lateral impact. *Eng. Struct.* **2023**, *280*, 115719. [[CrossRef](#)]
13. Ostrowski, K.; Dudek, M.; Sadowski, L. Compressive behaviour of concrete-filled carbon fiber-reinforced polymer steel composite tube columns made of high performance concrete. *Compos. Struct.* **2020**, *234*, 111668. [[CrossRef](#)]
14. Ostrowski, K.; Chastre, C.; Furtak, K.; Malazdrewicz, S. Consideration of critical parameters for improving the efficiency of concrete structures reinforced with FRP. *Materials* **2022**, *15*, 2774. [[CrossRef](#)] [[PubMed](#)]
15. Symonds, P.S. Survey of methods of analysis for plastic deformation of structures under dynamic Loading. *Ciência Technol. Aliment.* **1967**, *31*, 967–972.
16. Han, L.; Yao, G.; Tao, Z. Performance of concrete-filled thin-walled steel tubes under pure torsion. *Thin-Walled Struct.* **2007**, *45*, 24–36. [[CrossRef](#)]
17. Han, L.H. *Concrete-Filled Steel Tubular Structure: Theory and Practice*; Science Press: Beijing, China, 2007.
18. Forni, D.; Chiaia, B.; Cadoni, E. Strain rate behaviour in tension of S355 steel: Base for progressive collapse analysis. *Eng. Struct.* **2016**, *119*, 164–173. [[CrossRef](#)]
19. Reid, S.R.; Reddy, T.Y. Static and dynamic crushing of tapered sheet metal tubes of rectangular cross-section. *Int. J. Mech. Sci.* **1986**, *28*, 623–637. [[CrossRef](#)]
20. Abramowicz, W.; Jones, N. Dynamic progressive buckling of circular and square tubes. *Int. J. Impact Eng.* **1986**, *4*, 243–270. [[CrossRef](#)]
21. Tao, Z.; Wang, Z.; Yu, Q. Finite element modelling of concrete-filled steel stub columns under axial compression. *J. Constr. Steel Res.* **2013**, *133*, 121–131. [[CrossRef](#)]
22. CEB-FIP. *Concrete Structures under Impact and Impulsive Loading—Synthesis Report*; Comité Euro-International du Béton: Lausanne, Switzerland, 1988; Volume 187, 184p.
23. Yang, Y.F.; Zhang, Z.C.; Fu, F. Experimental and numerical study on square RACFST members under lateral impact loading. *J. Constr. Steel Res.* **2015**, *111*, 43–56. [[CrossRef](#)]
24. Jia, D.B. *Preliminary Study on Concrete-Filled Steel Tubular Members under Lateral Impact Load*; Taiyuan University of Technology: Taiyuan, China, 2005.
25. Gao, S.; Zhao, G.H.; Guo, L.H.; Zhou, L.Q.; Yuan, K.K. Utilization of coal gangue as coarse aggregates in structural concrete. *Constr. Build. Mater.* **2021**, *268*, 121212. [[CrossRef](#)]
26. Cai, S.H. *Contemporary Concrete-Filled Steel Tube Structure*; Beijing People's Traffic Press: Beijing, China, 2003.

**Disclaimer/Publisher's Note:** The statements, opinions and data contained in all publications are solely those of the individual author(s) and contributor(s) and not of MDPI and/or the editor(s). MDPI and/or the editor(s) disclaim responsibility for any injury to people or property resulting from any ideas, methods, instructions or products referred to in the content.